Deep–Sea Research II xx (xxxx) xxxx–xxxx

Contents lists available at ScienceDirect

Deep–Sea Research II

journal homepage: www.elsevier.com/locate/dsr2

Characteristics of the modelled meteoric freshwater budget of the western Antarctic Peninsula

J.M. van Wessem[a,*], M.P. Meredith[b], C.H. Reijmer[a], M.R. van den Broeke[a], A.J. Cook[c]

[a] Institute for Marine and Atmospheric Research Utrecht, Utrecht University, Utrecht, The Netherlands
[b] British Antarctic Survey, Cambridge, United Kingdom
[c] Department of Geography, Durham University, Durham, United Kingdom

ARTICLE INFO

Keywords:
Western Antarctic Peninsula
Climate
Freshwater budget
Ocean
Regional climate modelling

ABSTRACT

Rapid climatic changes in the western Antarctic Peninsula (WAP) have led to considerable changes in the meteoric freshwater input into the surrounding ocean, with implications for ocean circulation, the marine ecosystem and sea-level rise. In this study, we use the high-resolution Regional Atmospheric Climate Model RACMO2.3, coupled to a firn model, to assess the various contributions to the meteoric freshwater budget of the WAP for 1979–2014: precipitation (snowfall and rainfall), meltwater runoff to the ocean, and glacial discharge. Snowfall is the largest component in the atmospheric contribution to the freshwater budget, and exhibits large spatial and temporal variability. The highest snowfall rates are orographically forced and occur over the coastal regions of the WAP (>2000 mm water equivalent (w.e.) y^{-1}) and extend well onto the ocean up to the continental shelf break; a minimum (~500 mm w. e. y^{-1}) is reached over the open ocean. Rainfall is an order of magnitude smaller, and strongly depends on latitude and season, being large in summer, when sea ice extent is at its minimum. For Antarctic standards, WAP surface meltwater production is relatively large (> 50 mm w. e. y^{-1}), but a large fraction refreezes in the snowpack, limiting runoff. Only at a few more northerly locations is the meltwater predicted to run off into the ocean. In summer, we find a strong relationship of the freshwater fluxes with the Southern Annular Mode (SAM) index. When SAM is positive and occurs simultaneously with a La Niña event there are anomalously strong westerly winds and enhanced snowfall rates over the WAP mountains, Marguerite Bay and the Bellingshausen Sea. When SAM coincides with an El Niño event, winds are more northerly, reducing snowfall and increasing rainfall over the ocean, and enhancing orographic snowfall over the WAP mountains. Assuming balance between snow accumulation (mass gain) and glacial discharge (mass loss), the largest glacial discharge is found for the regions around Adelaide Island (10 Gt y^{-1}), Anvers Island (8 Gt y^{-1}) and southern Palmer Land (12 Gt y^{-1}), while a minimum (< 2 Gt y^{-1}) is found in Marguerite Bay and the northern WAP. Glacial discharge is in the same order of magnitude as the direct freshwater input into the ocean from snowfall, but there are some local differences. The spatial patterns in the meteoric freshwater budget have consequences for local productivity and carbon drawdown in the coastal ocean.

1. Introduction

During the second half of the twentieth century, the western Antarctic Peninsula (WAP) warmed more rapidly than any other region in the Southern Hemisphere. Since 1950, the lower atmosphere above the WAP warmed by 3 °C (King, 1994; Vaughan et al., 2003). This, in combination with increased ocean heat content (Schmidtko et al., 2014), led to the loss of multiple ice shelves (Cook and Vaughan, 2010), a retreat for 90% of its marine terminating glaciers (Cook et al., 2014, 2016), an increase in precipitation (Thomas et al., 2008), and the disappearance of most of the perennial sea ice (Stammerjohn et al., 2011). All these changes affect the freshwater input (sea-ice melt and meteoric water, the latter combining precipitation and glacial discharge) into the surrounding ocean, significantly influencing the ecosystem, and, ultimately, the WAP contribution to regional and global sea-level rise (Ivins et al., 2013; Rye et al., 2014). Rising atmospheric temperatures increase snow melt-rates and meltwater runoff into the ocean (Vaughan, 2006). Intrusion of warm Circumpolar Deep Water (CDW) originating from the Antarctic Circumpolar Current (ACC) onto and across the continental shelf has been identified as the main cause of glacial ice loss in the Amundsen Sea and likely in the Bellingshausen Sea (Martinson, 2012; Pritchard et al., 2012),

* Corresponding author.
E-mail address: j.m.vanwessem@uu.nl (J.M. van Wessem).

http://dx.doi.org/10.1016/j.dsr2.2016.11.001

Available online xxxx

culminating in the retreat and calving of marine terminating glaciers (Wouters et al., 2015; Cook et al., 2016). Together with the (partial) disintegration of WAP ice shelves, such as Wilkins Ice Shelf (Scambos et al., 2009), large icebergs are formed that drift across the open ocean, releasing freshwater into the ocean as they melt (Silva et al., 2006). Spatial and temporal changes in sea-ice volume will significantly alter ocean temperature, salinity and stratification in the vicinity of the WAP (Stammerjohn et al., 2008; Meredith et al., 2013). The marine ecology of the upper ocean adjacent to the WAP responds to these changes in the freshwater budget (Meredith and King, 2005): freshening of the upper ocean stabilizes the water column and enhances phytoplankton blooms (Montes-Hugo et al., 2009); it also alters the ocean circulation by changing the geostrophic flow (Martinson, 2012).

Measurements of stable isotopes of oxygen in seawater enable a quantitative separation of the contributions of sea-ice melt and meteoric water to the total freshwater budget (Meredith et al., 2008, 2010). Several studies used oxygen isotope data from the Palmer Long-Term Ecological Research programme (Pal-LTER; http://pal.lternet.edu/) and the Rothera Oceanographic and Biological Time Series (RaTS; Clarke et al., 2008), as part of more comprehensive suites of physical, biogeochemical and biological measurements (Fig. 1). Some of these studies have found that, as a result of the contributions of both glacial meltwater (Dierssen et al., 2002) and precipitation (Meredith et al., 2008), the meteoric water flux is the dominating freshwater source overall. However, a new study found that sea ice melt contributions can be comparable to the meteoric water flux in specific years because of the large interannual variability of the latter (Meredith et al., 2016).

It is thus clear that quantifying the spatial and temporal variability of the meteoric freshwater input is important for interpreting current and future changes in the WAP. Meteoric freshwater fluxes depend on atmospheric forcing, including the direction and magnitude of atmospheric water vapour transport (Meredith et al., 2010). The are linked to subannual and interannual climate variability as expressed in e.g. the Southern Annular Mode (SAM; Marshall, 2003; Thomas et al., 2008), and the El Niño/Southern Oscillation phenomenon (ENSO, Wolter and Timlin, 1993; Turner, 2004) and their interconnection (Clem and Fogt, 2013). Moreover, model studies have found that

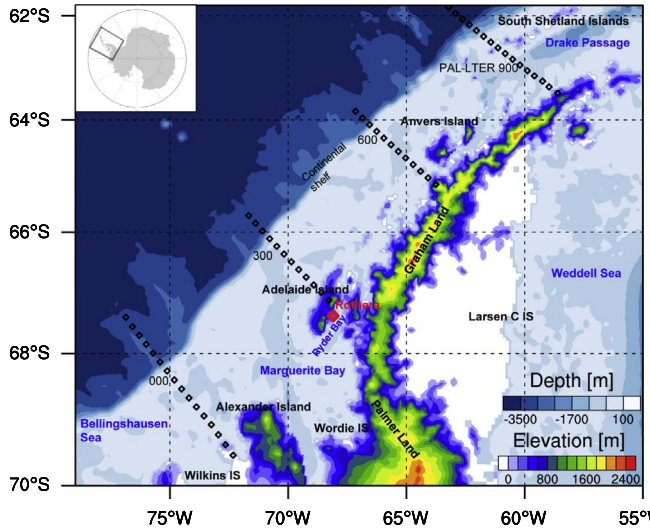

Fig. 1. The northern (> 70°S) Antarctic Peninsula (AP) domain (black box in inset map of Antarctica shows the full AP RACMO2.3 model domain and boundaries, which extends to 75°S) with model surface topography [m] and ocean depth [m] of the AP. White areas represent floating ice shelves and regions over land with elevations <40 m, colours represent the elevation of the grounded ice sheet and ocean depth. Locations of four transects are shown (black diamonds), coinciding with survey lines from the Pal-LTER program, as used in Section 3.1. Some locations as used througout the text are marked. (For interpretation of the references to color in this figure legend, the reader is referred to the web version of this article.)

precipitation rates over the WAP and the adjacent ocean are extremely high due to strong orographic uplift (Van Wessem et al., 2016). This affects both the direct (precipitation) and indirect (glacial discharge) meteoric freshwater fluxes. Partitioning the contributions of these fluxes is important as they affect the ecosystem in different ways: unlike precipitation, glacial discharge can transport micronutrients and trace metals such as iron to the ocean as the glaciers scour the underlying rock and sediment (Hawkings et al., 2014). However, making this distinction from observations is difficult, especially in the coastal areas where these fluxes are largest, as both water sources have a similar isotopic composition and can be comparable in magnitude (Meredith et al., 2013). An additional complication is the challenge of distinguishing basal melting from iceberg calving on the basis of ocean tracer data alone (Meredith et al., 2013).

Atmospheric models provide information about meteoric freshwater input, but are generally limited in horizontal resolution and hence do not resolve the large spatial variability of WAP precipitation rates (Van Wessem et al., 2014a), are limited in simulation length (Van Lipzig et al., 2004; Bromwich, 2004), or have limitations in their ability to resolve atmospheric and/or snow related processes (Nicolas and Bromwich, 2011). In this study, we use the newest version of the Regional Atmospheric Climate Model RACMO2.3 to address the above issues. The model is run at high horizontal resolution (5.5 km) to properly simulate the large spatial variability of the WAP topography and associated climate variables. The model separately simulates the WAP meteoric freshwater components of snowfall, rainfall and meltwater for the period 1979–2014. The model is forced with ERA-Interim, the most reliable re-analysis data for the Southern Ocean and troposphere (Bracegirdle and Marshall, 2012), and is coupled to a Firn Densification Model (FDM) that calculates processes in the snowpack such as the percolation and refreezing of meltwater; runoff into the ocean is assumed to occur instantaneously at the snow/ice interface (Ettema et al., 2010; Ligtenberg et al., 2011). Multiple studies evaluated the performance of RACMO2.3 by comparing model output to observational data; the model has been proven to realistically simulate the near-surface climate and surface mass balance of Antarctica (Van Wessem et al., 2014a,b), as well as that of the Antarctic Peninsula (Van Wessem et al., 2015, 2016). However, significant model biases remain: there is a cold surface bias related to uncertainties in cloud cover and its relation to short- and longwave radiation (Van Wessem et al., 2014a; King et al., 2015), and associated biases in the melt-fluxes and the interaction of melt in the snowpack (Kuipers Munneke et al., 2012; Barrand et al., 2013b). However, as we have shown in Van Wessem et al. (2016), Antarctic Peninsula melt rates are small compared to the other freshwater fluxes, and these biases do not strongly influence the modelled freshwater budget. First, in Section 2, we introduce the model and methods used. In Sections 3.1 and 3.2 we discuss the spatial and temporal variability of the meteoric freshwater components, and present an indirect estimate of WAP glacial discharge in Section 3.3, based on long-term average surface mass balance fields and detailed glacier catchment outlines. Finally, we discuss the results and present conclusions in Section 4.

2. Methods

2.1. RACMO2.3 and FDM

We use the hydrostatic Regional Atmospheric Climate Model RACMO2.3. Model settings are similar to Van Wessem et al. (2016). We only discuss model output north of 70°S, even though the simulations were conducted for a domain extending as far south as 75°S, in order to focus specifically on the WAP areas that include the RaTS and Pal-LTER field sites. We included Larsen B ice shelf in the model domain, even though it has collapsed during the period of the model run, and will discuss the results accordingly. All further model details and a thorough evaluation of model results are described in Van

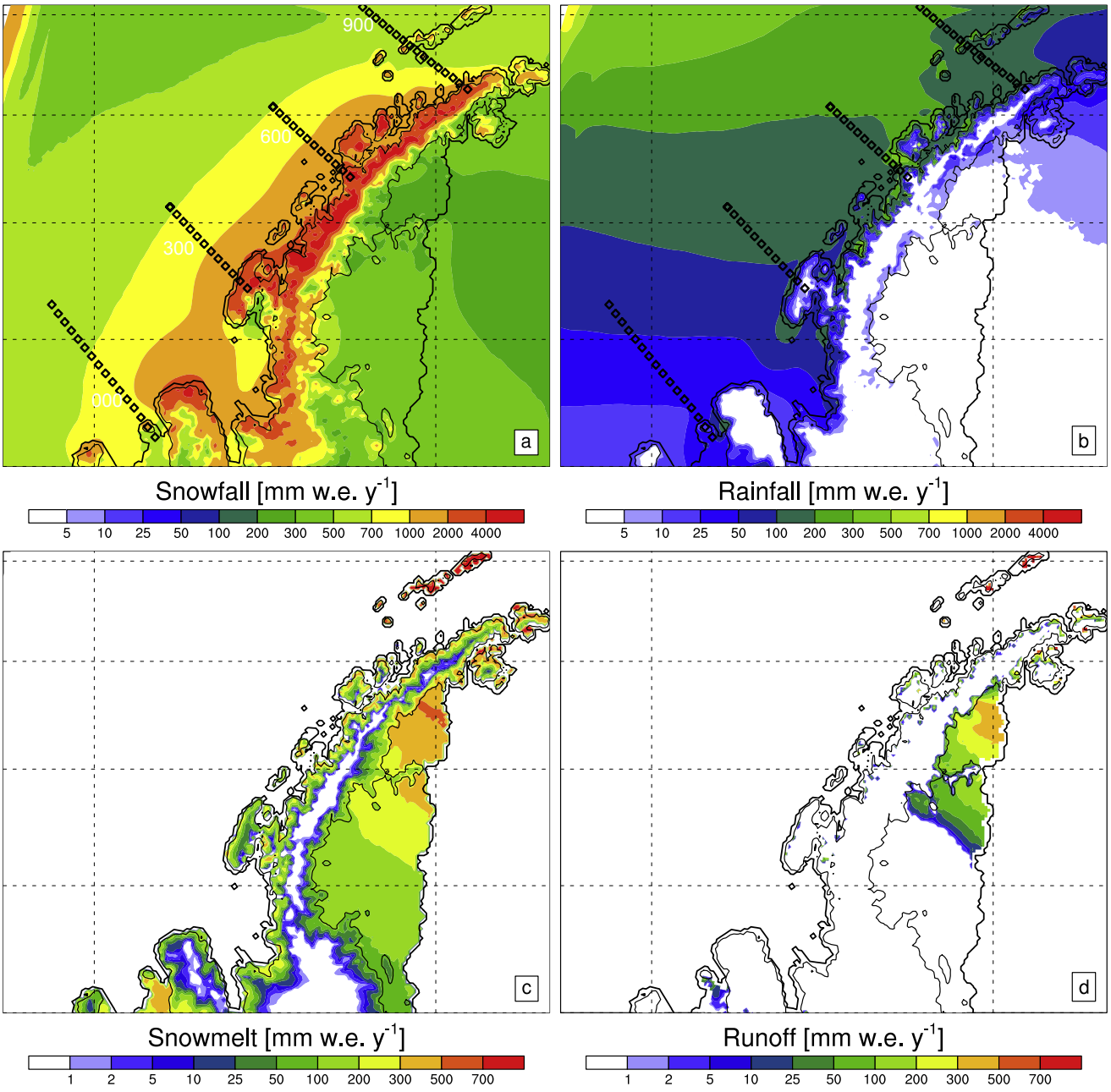

Fig. 2. Climatological (1979–2014) freshwater fluxes from RACMO2.3: snowfall (a), rainfall (b), snowmelt (c) and meltwater runoff (d) in mm w. e. y^{-1}. Note the different scales in a,b compared to c,d. Also shown in a,b are the Pal-LTER transects as used in this study.

Wessem et al. (2014a, 2015, 2016).

RACMO2.3 is coupled to a FDM, a single column time-dependent model that describes the evolution of the firn layer. It calculates firn density, temperature and liquid water content evolution based on forcing at the surface by RACMO2.3 surface temperature, accumulation and wind speed at 3 hourly resolution. The firn layer has great spatial variability and has firn depths >100 m in high accumulation regions. Surface meltwater percolates into the model firn layer, where it can refreeze, be stored or percolate further down. The retention of meltwater is based on the 'tipping-bucket' method (i.e. liquid water is stored in the first available layer and transported downwards only when it exceeds the maximum capillary retention). Liquid water that reaches the bottom of the firn layer is removed as runoff. More details on the FDM can be found in Ligtenberg et al. (2011) and Kuipers Munneke et al. (2015).

2.2. SAM and ENSO

To analyse temporal variations in the meteoric freshwater budget, we analyse its sensitivity to the two leading modes of variability in the WAP region, i.e. the Southern Annular Mode (SAM) and El Niño/Southern Oscillation (ENSO). SAM is the leading mode of extratropical climate variability in the southern hemisphere, defined as the meridional pressure difference between a node centered over Antarctica and an annulus overlying the lower latitudes, and is associated with the intensity of the westerly winds impinging on the WAP (Thompson, 2002). ENSO variability originates in the tropical Pacific Ocean where it is most manifest, with changes in sea surface temperature (SST) on timescales 4–7 years; this variability reaches locations at high southern latitudes through both atmospheric and oceanic teleconnections (Yuan, 2004; Turner, 2004). We have selected the upper/lower quartiles (75%/25% percentiles) of monthly summer (December, January,

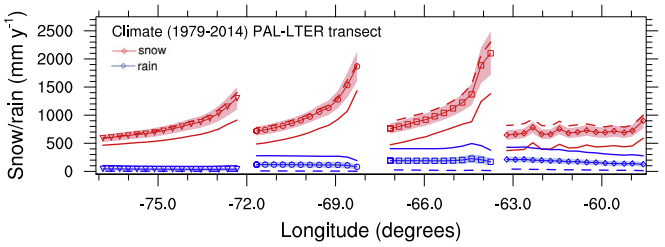

Fig. 3. Climatological (1979–2014) snowfall (red) and rainfall (blue) (mm w. e. y^{-1}) across Pal-LTER transects (see Figs. 1 and 2) 900 (diamonds), 600 (squares), 300 (circles) and 000 (triangles). Shading denotes interannual variability (one standard devation). The dashed lines denote the winter (Jun., Jul., Aug.) averages, the solid (unmarked) lines the summer (Dec., Jan., Feb.) averages. Each of the transects is extrapolated so as to include two land points. (For interpretation of the references to color in this figure legend, the reader is referred to the web version of this article.)

February (DJF)) indices from the Marshall (2003) SAM index (SAM ±) and Wolter and Timlin (1993) ENSO index (ENSO ± , where a positive index corresponds with El Niño conditions) series. The percentile thresholds are chosen such that the SAM/ENSO ± composites include ~10 months. We have specifically chosen to analyse summer months, even though ENSO weakly correlates with summer conditions in the AP (Clem and Fogt, 2013), given its importance for the freshwater fluxes (see Section 3.2). We then extracted the average model output for the corresponding months, and, to account for possible interconnections between SAM and ENSO, constructed SAM ± /ENSO ± composite maps of the relevant freshwater components, and discuss temporal extremes in these variables by comparing them with the 1979–2014 climatology.

2.3. Glacier catchments and meteoric freshwater budget

We calculated the average and integrated surface mass balance (SMB) for 676 glacier basins using delineations from Cook et al. (2014), to estimate glacial discharge of the WAP. We assume that, as the majority of glaciers are retreating and their retreat rates have recently accelerated (Pritchard et al., 2009; Cook et al., 2014, 2016), the minimum glacial discharge equals the average long-term SMB; the ice sheet is in steady state (ice discharge+SMB=0). We furthermore assume that the SMB averaged over the length of the model run (1979–2014) is representative of the recent glacier history of the WAP. We separately calculate the SMB for all basins that are larger than the size of one grid box (~30 km^2), including all grid points that are within the basin outline for at least 50% of the gridbox area. Because of the multitude of basins in this data-set, we binned the data into 27 0.25° latitudinal intervals from 70° to 63.25°S, based on the average latitude of the respective basin. In addition, to compare with glacial discharge, we calculated the average freshwater input into the ocean by precipitation (snowfall and rainfall). We integrated these fluxes over all WAP ocean grid-boxes up to the continental shelf (Fig. 1) and binned them into the above latitudinal intervals.

3. Results

3.1. Precipitation and snowmelt

Fig. 2 shows maps of the modelled average meteoric freshwater budget components. These will only be briefly discussed here; a more detailed description of AP climate is provided in Van Wessem et al. (2016). Fig. 2a shows large snowfall rates over the western AP and the adjacent ocean, due to orographic uplift. Up to 2000 mm water equivalent (w.e.) y^{-1} of snow falls over the ocean, decreasing steadily to the west, reaching 300 mm w. e. y^{-1} in the more distant ocean around the continental shelf break. Over the western mountain range, snowfall rates reach up to 5000 mm w. e. y^{-1}, resulting in annual snow layers >10 m deep. In Marguerite Bay snowfall rates are variable, being surrounded by the mountain ranges of Alexander Island, Adelaide Island and Palmer Land. The precipitation shadow of Adelaide Island is most pronounced, with dry conditions (~200 mm w. e. y^{-1}) over Ryder Bay. Here, snowfall and rainfall (Fig. 2b) rates are similar in magnitude; in most other locations rainfall is an order of magnitude smaller than snowfall or zero. In sharp contrast with the spatial variability of snowfall, which is mainly controlled by topography, gradients in rainfall are controlled by latitude and elevation. Moreover, while snowfall occurs all year, rainfall is mostly restricted to summer, when sea-ice extent is at its minimum. Therefore, summer rainfall has a relatively large contribution to the freshwater flux into the ocean. However, snowfall that accumulates on sea ice in winter, melts with the sea ice in spring/summer, and at these locations the snowfall freshwater flux to the ocean is delayed.

Surface snowmelt (Fig. 2c) is widespread over the WAP with sharp latitudinal and elevation gradients. Meltwater has the potential to result in runoff into the ocean when the firn layer has insufficient refreezing capacity (Kuipers Munneke et al., 2014). Fig. 2d shows that this rarely happens over the WAP; only in lower-lying regions with low accumulation rates, and high meltwater production, does some local meltwater runoff occur. Runoff is more frequent over Larsen B and C ice shelves in the eastern AP (EAP) and on Wilkins ice shelf farther south.

Fig. 3 shows modelled climatological and seasonal snowfall and rainfall rates along four Pal-LTER transects. Along the four transects, average snowfall rates over the ocean are roughly comparable (~500 mm w. e. y^{-1}), and all peak towards the coast due to the orographic effect. Higher peak values are found for the 300 and 600 transects, with a maximum >2000 mm w. e. y^{-1} for the 600 transect. While for transects 000, 300 and 600 snowfall rates rapidly decrease towards the west, snowfall is low and constant in magnitude over the entire 900 transect. This is related to the more northerly oriented slopes, which, in combination with westerly winds, results in weaker orographic precipitation. Moreover, in contrast to the other transects, the 900 transect shows an increase of rainfall towards the northwest. Interannual variability (the red and blue shading) is closely related to the absolute magnitude and does not show a relation with the location along the transect, a feature that was also reported in Van Wessem et al. (2016).

It is important to note the seasonal precipitation cycle. Fig. 3 shows that summer snowfall, when the westerly circulation is weaker, is smaller than winter snowfall by ~400 mm w. e. y^{-1} for all transects; this effect exceeds the interannual variability of ~100 mm w. e. y^{-1}. As a result, the relative/fractional contribution of rainfall is large in summer: for transects 900 and 600 rainfall reaches summer values that are almost as large or even larger than that of snowfall, further emphasizing the importance of rainfall for the summertime meteoric freshwater budget of the WAP.

No significant trends in any of the freshwater budget components for any of the transects were found for the period 1979–2014, except for small negative trends in rainfall near the coast that are related to cooling trends over the mountain slopes as reported in Van Wessem et al. (2015).

3.2. SAM and ENSO climate variability

Temporal variability in the WAP freshwater budget has a strong relation to the magnitude and the interconnection of both the circumpolar westerlies and forcing from the tropics, which is reflected in variability associated with both SAM and ENSO, respectively (Fogt et al., 2011; Clem and Fogt, 2013). We present composite maps (SAM/ENSO ± , see Section 2.2) of the meteoric freshwater fluxes and compare them to the 1979–2014 climatology. We specifically provide maps based on summer (DJF) months, even though snowfall rates are higher in winter and ENSO shows a weak relation to summer

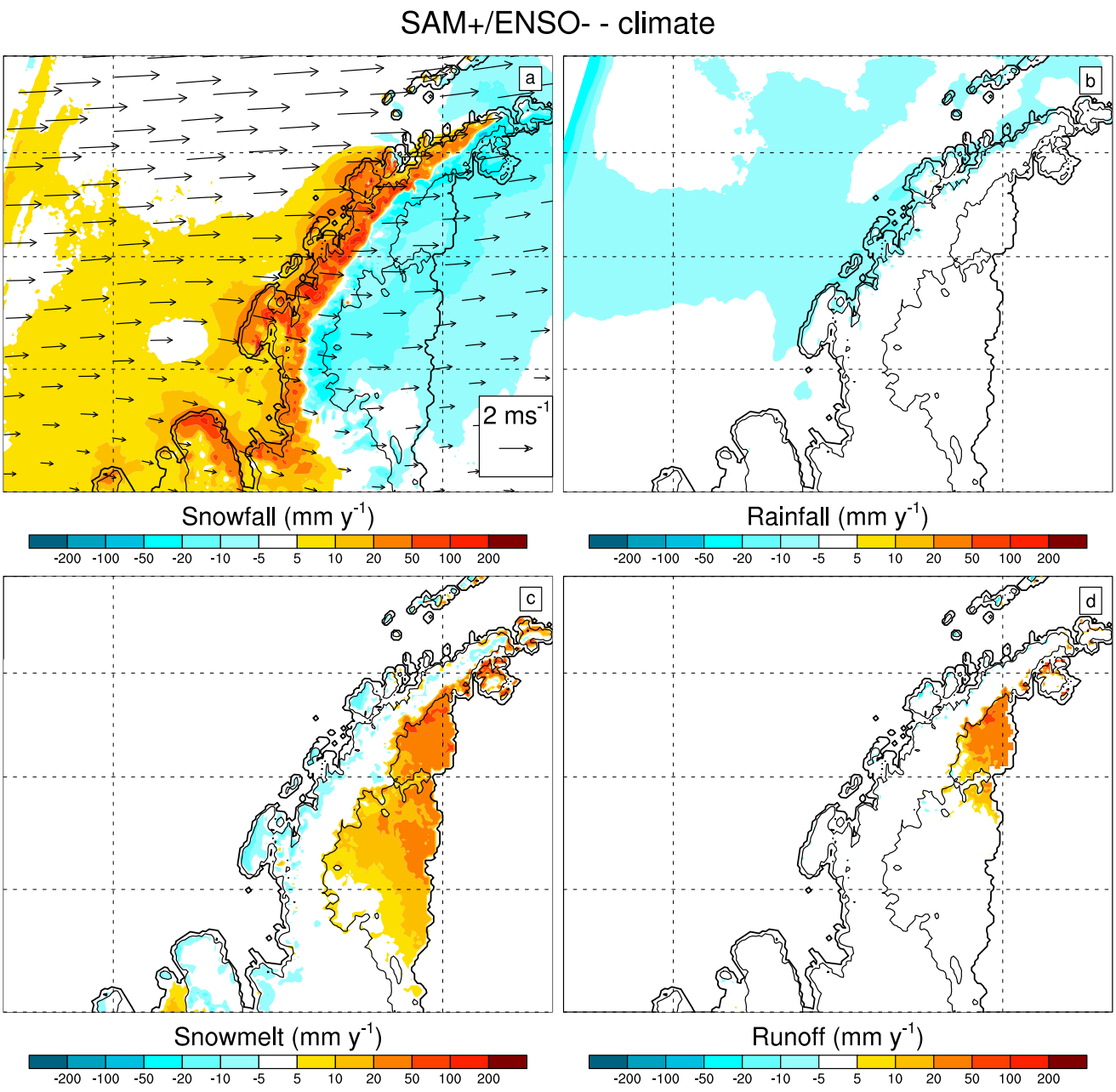

Fig. 4. Difference of the SAM^{+}/ENSO^{-} composite with the climatology (1979–2014) of the summer months (Dec., Jan., Feb.) freshwater components snowfall (a), rainfall (b), snowmelt (c) and meltwater runoff (d), in mm w. e. y^{-1} for 1979–2014. In (a) 500 hPa wind speed difference vectors are also shown. Details are found in Section 2.2.

conditions, because most snow falls on the sea ice and melts in summer, and because of the relative importance of summer compared to winter of the other fluxes (Section 3.1).

Fig. 4 shows the freshwater flux anomalies, when the indices are in-phase (SAM+ occurs during La Niña) and the ENSO connection to the AP region is stronger than average (following Fogt et al., 2011; Clem and Fogt, 2013): when SAM is high westerly circulation is anomalously strong and persistent over the region, enhancing topographic precipitation in the WAP and reducing it in the precipitation shadow of the AP spine. This is clearly shown in Fig. 4a: during SAM^{+} snowfall rates are highly elevated over the mountains (~100 mm w. e. y^{-1}), slightly elevated over the adjacent ocean (~20 mm w. e. y^{-1}), and reduced by ~20 mm w. e. y^{-1} in the EAP. In the WAP, even though snowfall is higher during SAM+/ENSO−, rainfall is slightly lower, which is related to enhanced convection and associated cooling, explaining the relatively low WAP warming compared to the EAP during SAM+ (Marshall et al., 2006; van Lipzig et al., 2008). Snowmelt dependency on SAM shows distinct patterns, with a negative anomaly to the west, and a positive anomaly to the east, which is also consistent with earlier studies (Marshall et al., 2006). This anomaly is a result of warm downslope winds, enhancing melt especially over the ice shelves. Consequently, runoff fluxes are high over the EAP ice shelves during SAM+/ENSO−.

Fig. 5 shows the freshwater flux anomalies, when the indices are out of phase (SAM+ occurs during El Niño) and the ENSO connection to the AP region is relatively weak (Clem and Fogt, 2013). Here, the westerly wind anomaly includes a stronger northerly component and the winds are more perpendicular to the mountain range, enhancing the topographic snowfall further (> 200 mm w. e. y^{-1}). Moreover, the northwesterly winds advect warm air towards the WAP, enhancing rainfall and reducing snowfall over the Bellingshausen Sea. In addition, the warmer air results in a positive snowmelt anomaly in the WAP, and enhances the positive EAP snowmelt/runoff anomalies. An additional interesting feature is that during SAM+/ENSO- the wind anomaly

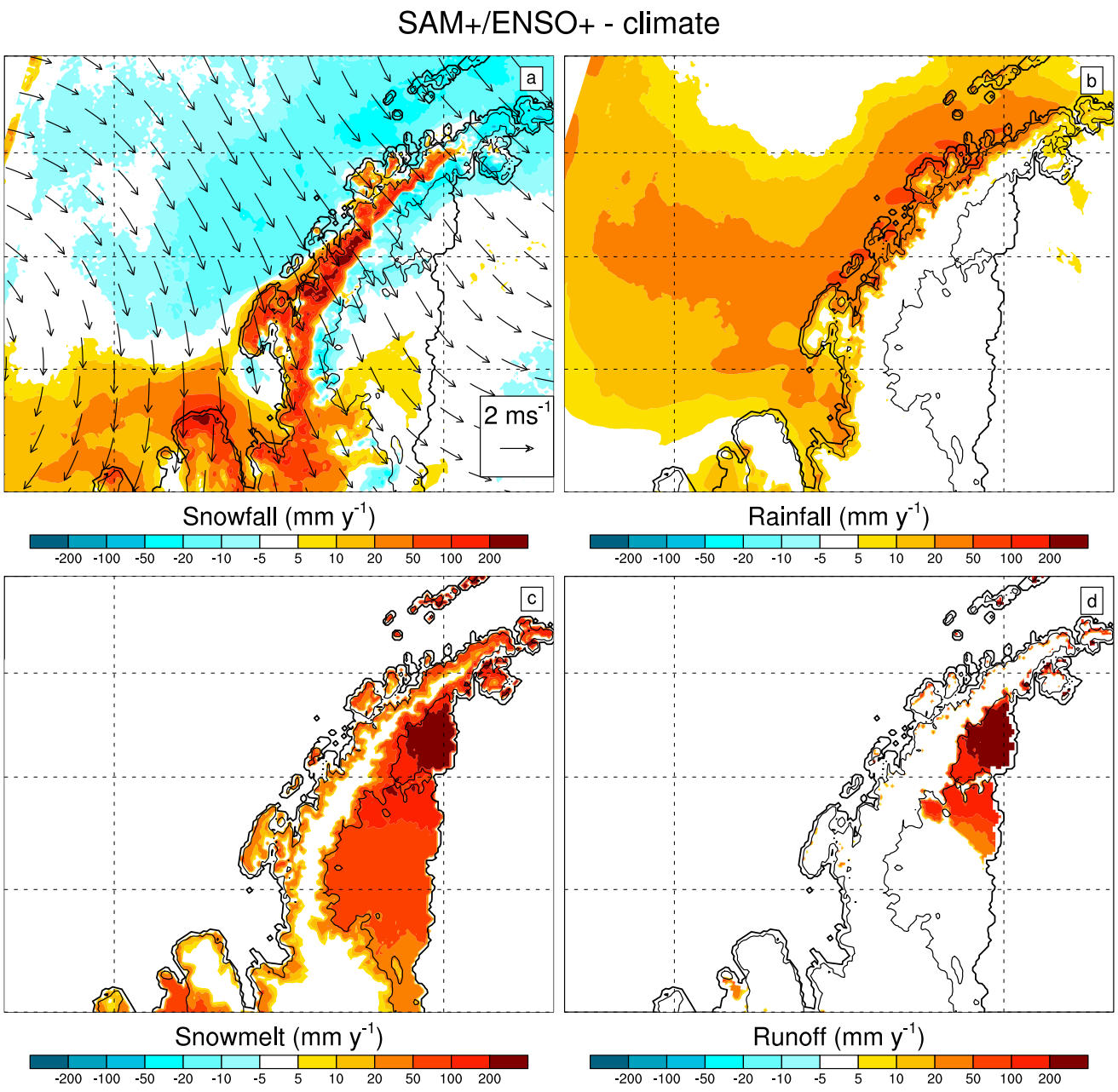

Fig. 5. Difference of the SAM^{+}/ENSO^{+} composite with the climatology (1979–2014) of the summer months (Dec., Jan., Feb.) freshwater components snowfall (a), rainfall (b), snowmelt (c) and meltwater runoff (d), in mm w. e. y^{-1} for 1979–2014. In a) 500 hPa wind speed difference vectors are also shown. Details are found in Section 2.2.

blows into Marguerite Bay and Ryder Bay, enhancing snowfall, while during SAM+/ENSO+ snowfall is reduced in Ryder Bay and parts of Marguerite Bay because it is in the precipitation shadow of Adelaide Island, showing that this region is particularly sensitive to varying atmospheric conditions. To further analyse the specific influence of ENSO, we have looked at neutral and low values of the SAM indices, but found these results to be inconclusive, likely due to the insignificant correlation of ENSO with the WAP in summer (Clem and Fogt, 2013).

3.3. Glacial discharge and the meteoric freshwater budget

Fig. 6 shows modelled climatological (1979–2014) specific surface mass balance (SSMB) and the estimated meteoric freshwater budget: area integrated SMB and runoff for WAP glacier basins, and ocean area integrated snowfall and rainfall. Over the grounded WAP ice sheet, SSMB is defined as the area averaged surface mass balance (SMB). Average and integrated SMB and runoff are calculated for all WAP glacier basins defined by Cook et al. (2014). The freshwater fluxes are binned into 27 latitudinal intervals of 0.25°, ranging from 70° to 63.25°S. Average and integrated snowfall and rainfall are computed over all WAP ocean grid-boxes in the latitudinal bins up to the continental shelf. First, the SSMB shows large latitudinal variability, with a clear maximum between 66.25° and 65.75°S, where SSMB >5 m w. e. y^{-1}, coinciding with the region of largest snowfall rates, just north of Adelaide Island (Fig. 2a). In this region WAP surface elevation is the largest, resulting in efficient orographic precipitation. The minimum SSMB is found in southern Palmer Land, with values ~1 m w. e. y^{-1}. The barplot in the left panel of Fig. 6 shows the SMB and meltwater runoff, integrated over the glacier basins, and snowfall and rainfall, integrated over the ocean. We assume that the average SMB over the length of the model run (36 years) is in steady state with glacial discharge, providing a rough estimate of glacial discharge along the WAP coast. Recent studies (Cook et al., 2014, 2016) found that ~90% of WAP glaciers, and several northern AP glaciers (Scambos

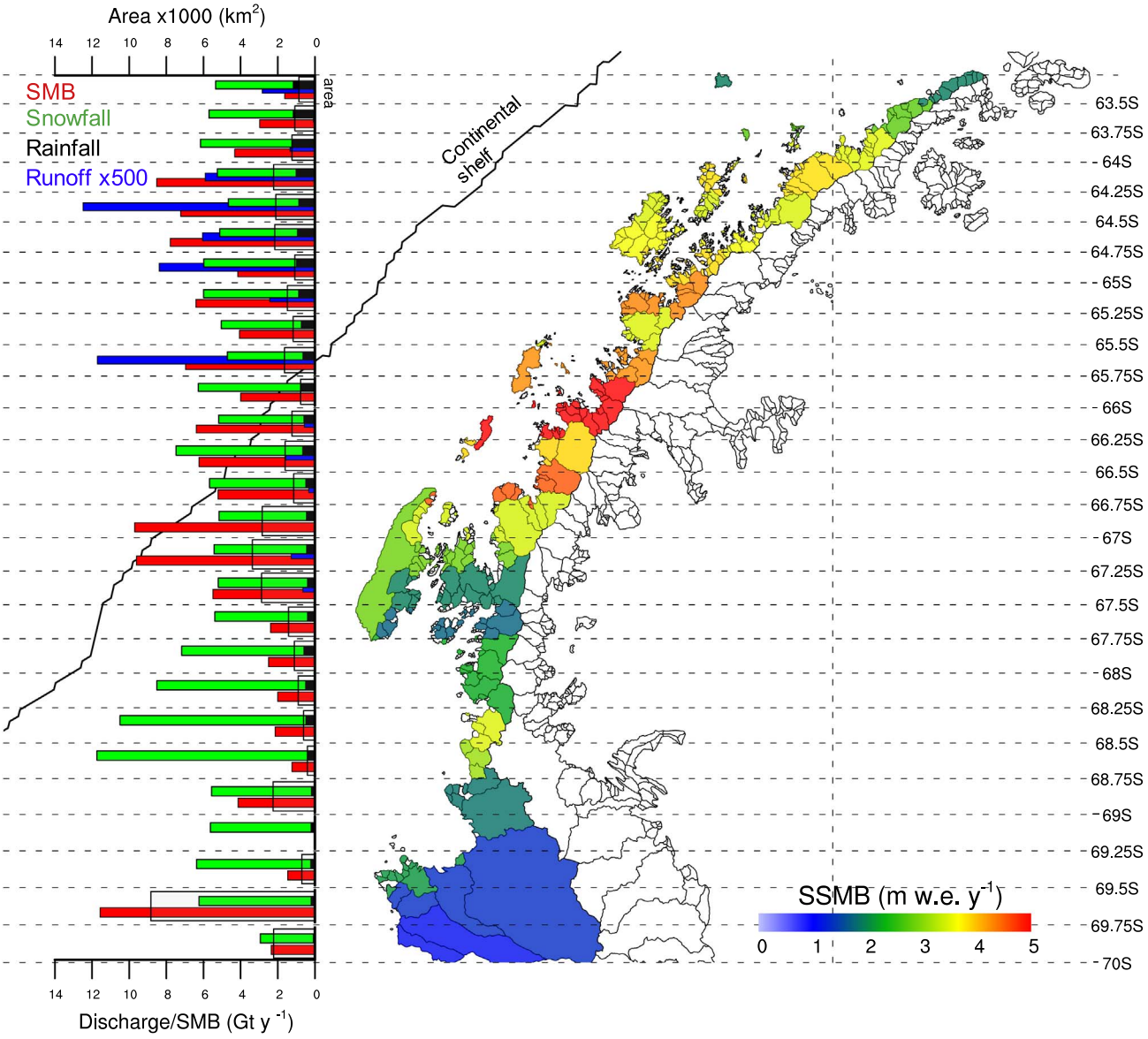

Fig. 6. Specific (area averaged) surface mass balance (SSMB; m w. e. y^{-1}; colours), basin integrated SMB (Gt y^{-1}; red bars), meltwater runoff (500·Gt y^{-1}; blue bars), ocean integrated snowfall/rainfall (Gt y^{-1}; green/black bars) and area (1000 km^2; black boxes) binned into 27 latitudinal intervals (0.25°). Only WAP basins larger than the area of one gridbox are used. Basin definitions are based on Cook et al. (2014). For each basin, the average latitude is calculated, which is used to determine to which bin the basin belongs. Ocean basins are based on all gridboxes up to the continental shelf (black line; see Fig. 1). (For interpretation of the references to color in this figure legend, the reader is referred to the web version of this article.)

et al., 2014), are retreating, especially to the south where retreat is strongest (Cook et al., 2014). This implies that the average SMB likely provides a lower estimate of glacial discharge. However, the timescale of AP glacial discharge can be longer than the length of the model run (Barrand et al., 2013a). Therefore, real discharge rates can also be lower than estimated for glacier basins with longer discharge time-scales, as large trends in WAP accumulation are found in decades prior to 1979 (Thomas et al., 2008). The integrated snowfall and rainfall fluxes complete the meteoric freshwater budget. We assume, as a first order estimate, that these fluxes, together with glacial discharge, are redistributed in the adjacent WAP ocean. In reality the AP coastal current (Moffat et al., 2008) will transport the freshwater components southwards.

We find the highest basin-integrated SMB, and therefore the highest estimated glacial discharge, in the 70°–69.5°S bins. Even though SSMB was lowest here, this bin has by far the largest area (8000 km^2), and ~12 Gt y^{-1} of ice is discharged into the ocean; at these high latitudes all surface meltwater refreezes, and runoff is zero. Moving north, in the Marguerite Bay glacier basins (69°–67.75°S), basin discharge ranges from 1.5 to 4 Gt y^{-1}; in the Adelaide Island bins (67.25°–66.75°S), area and glacial discharge peak are 4000 km^2 and 11 Gt y^{-1}, respectively. Here, we also find the southernmost bin with significant modelled runoff, but values are typically three orders of magnitude smaller than SMB, and largely negligible. In the bins with the highest SSMB (bins 66.25° and 65.75°S), the basins are relatively small (< 2000 km^2) and discharge is lower (< 6 Gt y^{-1}). The largest SMB for the northwestern AP is found between 65° and 64°S, the location of Anvers Island, with values up to 8 Gt y^{-1}. Finally, in the northernmost bins, discharge decreases to ~2 Gt y^{-1}; a result of the small basin area and the relatively low SSMB (1–2 m w. e. y^{-1}).

In most bins the integrated snowfall fluxes have the same order of magnitude as glacial discharge; evidently rainfall fluxes are small and increase in magnitude towards the north, with the highest values up to 20% that of snowfall. There are some locations where the snowfall fluxes show larger differences with discharge: in the southern bins up to 67.5°S integrated snowfall fluxes are significantly larger (~12 Gt y^{-1}) than discharge, except for the 69.75°–69.5°S bin, where the glacier catchment area is the largest. This is due to both the small glacier

basins and the (nearly linear) increasing distance to the continental shelf and increasing ocean area (no fluxes are computed for Alexander Island). Towards the north, the bins near Adelaide Island stand out where discharge is twice as large as snowfall. Finally, in the two northernmost bins, where SSMB and SMB are both small, integrated snowfall is larger than discharge.

4. Summary and conclusions

The climate and associated freshwater budget of the western Antarctic Peninsula (WAP) is changing rapidly, with significant consequences for the surrounding ocean, atmosphere and ecosystem. Here, we use the Regional Atmospheric Climate Model RAMCO2.3, for the period 1979–2014, to interpret temporal and spatial variability in the meteoric freshwater budget: precipitation, meltwater runoff and glacial discharge. We find that snowfall is the largest component in the atmospheric contribution to the meteoric freshwater budget. It shows large spatial and seasonal variability, with average snowfall rates over the grounded ice sheet >2000 mm w. e. y^{-1} due to orographic uplift of moist air over the steep AP mountain range, decreasing to ~500 mm w. e. y^{-1} over the open ocean. Rainfall is an order of magnitude smaller than snowfall, and is mainly determined by temperature, altitude and latitude. However, because rainfall is highest in summer, when it is not intercepted by sea ice that is at its minimum, the contribution of rainfall to the freshwater flux into the ocean is relatively large, and at lower latitudes nearly as large as that of snowfall. The WAP meltwater production is large compared to the rest of the Antarctic continent (> 50 mm w. e. y^{-1}), but most meltwater refreezes in the cold snowpack; only at a few locations does meltwater run off into the ocean, and this contribution to the freshwater budget is small.

Temporal variability of the freshwater components is related to the Southern Annular Mode (SAM) and El Niño/Southern Oscillation (ENSO) indices. In summer, we find a strong relationship of the freshwater fluxes with SAM, and a weak relation with ENSO. When high index states of SAM coincide with La Niña events, snowfall is enhanced over Marguerite Bay and the Bellingshausen Sea. Over the WAP orographic precipitation is enhanced and snowmelt reduced. When SAM occurs during an El Niño event, winds are more northwesterly transporting warmer air to the WAP, resulting in reduced snowfall and enhanced rainfall over the ocean.

Finally, we use long-term average (1979–2014) modelled surface mass balance (SMB) to provide a rough estimate of glacial discharge. We find strong latitudinal differences, with peak values in the regions around Adelaide Island (10 Gt y^{-1}), Anvers Island (8 Gt y^{-1}) and southern Palmer Land (12 Gt y^{-1}). Minima (< 2 Gt y^{-1}) are found in Marguerite Bay and the northern WAP. As there is a net mass loss of the majority of WAP glaciers, these estimates based on SMB likely represent a lower limit for discharge. At most locations these fluxes are in the same order of magnitude as the integrated snowfall fluxes into the ocean. Integrated rainfall fluxes are an order of magnitude lower, peaking in the north.

The results of this study can, among other applications, be used to improve the interpretation of seawater isotope datasets, as from such observations alone one cannot readily distinguish between the different meteoric freshwater components, often combining precipitation and glacial discharge fluxes as a single contribution. A remaining challenge is a further partitioning of the glacial discharge flux into the contributions made by basal melting and calving of icebergs.

Acknowledgements

This study is funded by the Netherlands Polar Program (NPP) and the Netherlands Organization of Scientific Research, section earth and Life Sciences section (NWO/ALW).

References

Barrand, N.E., Hindmarsh, R.C.A., Arthern, R.J., Williams, C.R., Mouginot, J., Scheuchl, B., Rignot, E., Ligtenberg, S.R.M., Van Den Broeke, M.R., Edwards, T.L., Cook, A.J., Simonsen, S.B., 2013a. Computing the volume response of the Antarctic Peninsula ice sheet to warming scenarios to 2200. J. Glaciol. 59 (215), 397–409, (URL ⟨http://www.igsoc.org/journal/59/215/t12J139.html ⟩).

Barrand, N.E., Vaughan, D.G., Steiner, N., Tedesco, M., Kuipers Munneke, P., Van den Broeke, M.R., Hosking, J.S., 2013b. Trends in Antarctic Peninsula surface melting conditions from observations and regional climate modeling. J. Geophys. Res.: Earth Surf. 118 (1), 315–330, (URL http://doi.wiley.com/10.1029/2012JF002559).

Bracegirdle, T.J., Marshall, G.J., 2012. The reliability of antarctic tropospheric pressure and temperature in the latest global reanalyses. J. Clim. 25, 7138–7146.

Bromwich, D.H., 2004. Antarctic precipitation. Part I: spatial and temporal variability. J. Clim., 427–448.

Clarke, A., Meredith, M.P., Wallace, M.I., Brandon, M.A., Thomas, D.N., 2008. Seasonal and interannual variability in temperature, chlorophyll and macronutrients in northern Marguerite Bay, Antarctica. Deep Sea Res. Part II: Top. Stud. Oceanogr. 55 (18–19), 1988–2006, (URL ⟨http://www.sciencedirect.com/science/article/pii/S0967064508001537 ⟩).

Clem, K.R., Fogt, R.L., 2013. Varying roles of ENSO and SAM on the Antarctic Peninsula climate in austral spring. J. Geophys. Res.: Atmos. 118 (October), (n/a–n/a. URL ⟨http://doi.wiley.com/10.1002/jgrd.50860⟩).

Cook, A.J., Holland, P.R., Meredith, M.P., Murray, T., Luckman, A., Vaughan, D.G., 2016. Ocean forcing of glacier retreat in the western Antarctic Peninsula. Science 353 (6296), 1261–1273.

Cook, A.J., Vaughan, D.G., 2010. Overview of areal changes of the ice shelves on the Antarctic Peninsula over the past 50 years. Cryosphere 4 (1), 77–98, (URL ⟨http://www.the-cryosphere.net/4/77/2010/⟩).

Cook, A.J., Vaughan, D.G., Luckman, A.J., Murray, T., 2014. A new Antarctic Peninsula glacier basin inventory and observed area changes since the 1940s. Antarct. Sci. 26 (06), 614–624, (URL ⟨http://www.journals.cambridge.org/abstract_S0954102014000200 ⟩).

Dierssen, H. M., Smith, R. C., Vernet, M., 2002. Glacial meltwater dynamics in coastal waters west of the Antarctic peninsula. In: Proceedings of the National Academy of Sciences of the United States of America 99 (4), pp. 1790–1795 (URL < Go to ISI > ://WOS:000174031100010nnhttp://www.ncbi.nlm.nih.gov/pmc/articles).

Ettema, J., Van den Broeke, M.R., Van Meijgaard, E., Van de Berg, W.J., Box, J.E., Steffen, K., 2010. Climate of the Greenland ice sheet using a high-resolution climate model Part 1: evaluation. Cryosphere 4 (4), 511–527, (URL ⟨http://www.the-cryosphere.net/4/511/2010/⟩).

Fogt, R.L., Bromwich, D.H., Hines, K.M., 2011. Understanding the SAM influence on the South Pacific ENSO teleconnection. Clim. Dyn. 36 (7–8), 1555–1576, (URL ⟨http://link.springer.com/10.1007/s00382-010-0905-0 ⟩).

Hawkings, J.R., Wadham, J.L., Tranter, M., Raiswell, R., Benning, L.G., Statham, P.J., Tedstone, A., Nienow, P., Lee, K., Telling, J., 2014. Ice sheets as a significant source of highly reactive nanoparticulate iron to the oceans. Nat. Commun. 5, 3929, (URL ⟨http://www.nature.com/ncomms/2014/140521/ncomms4929/full/ncomms4929.html ⟩).

Ivins, E.R., James, T.S., Wahr, J., Schrama, O., Ernst, J., Landerer, F.W., Simon, K.M., 2013. Antarctic contribution to sea level rise observed by GRACE with improved GIA correction. J. Geophys. Res.: Solid Earth 118 (6), 3126–3141, (URL http://doi.wiley.com/10.1002/jgrb.50208).

King, J.C., 1994. Recent climate variability in the vicinity of the Antarctic Peninsula. Int. J. Climatol. 14 (1987), 357–369.

King, J.C., Gadian, A., Kirchgaessner, A., Kuipers Munneke, P., Orr, A., Reijmer, C., Broeke, M.R., Van Wessem, J.M., Weeks, M., 2015. Validation of the summertime surface energy budgetof Larsen C Ice Shelf (Antarctica) as represented in three high-resolution atmospheric models. J. Geophys. Res.: Atmos. 120 (4), 1335–1347.

Kuipers Munneke, P., Ligtenberg, S.R.M., Noël, B.P.Y., Howat, I.M., Box, J.E., Mosley-Thompson, E., McConnell, J.R., Steffen, K., Harper, J.T., Das, S.B., van den Broeke, M.R., 2015. Elevation change of the Greenland ice sheet due to surface mass balance and firn processes, 1960–2013. Cryosphere Discuss. 9 (3), 3541–3580, (URL ⟨http://www.the-cryosphere-discuss.net/9/3541/2015/tcd-9-3541-2015.html ⟩).

Kuipers Munneke, P., Ligtenberg, S.R.M., Van Den Broeke, M.R., Vaughan, D.G., 2014. Firn air depletion as a precursor of Antarctic ice-shelf collapse. J. Glaciol. 60 (220), 205–214, (URL ⟨http://www.igsoc.org/journal/60/220/t13J183.html ⟩).

Kuipers Munneke, P., Picard, G., van den Broeke, M.R., Lenaerts, J.T.M., van Meijgaard, E., 2012. Insignificant change in Antarctic snowmelt volume since 1979. Geophys. Res. Lett. 39 (1), 6–10, (URL ⟨http://www.agu.org/pubs/crossref/2012/2011GL050207.shtml ⟩).

Ligtenberg, S.R.M., Helsen, M.M., van den Broeke, M.R., 2011. An improved semi-empirical model for the densification of Antarctic firn. Cryosphere 5 (4), 809–819, (URL ⟨http://www.the-cryosphere.net/5/809/2011/ ⟩).

Marshall, G., Orr, A., Van Lipzig, N., King, J., 2006. The impact of a changing southern hemisphere annular mode on Antarctic Peninsula summer temperatures. J. Clim. 19 (2001), 5388–5404.

Marshall, G.J., 2003. Trends in the Southern annular mode from observations and reanalyses. J. Clim. 16 (24), 4134–4143, (URL ⟨http://journals.ametsoc.org/doi/full/10.1175/1520-0442(2003)(016%3C4134%3ATITSAM%3E2.0.CO;2⟩).

Martinson, D.G., 2012. Antarctic circumpolar current's role in the Antarctic ice system:

an overview. Palaeogeogr. Palaeoclim. Palaeoecol. 335–336, 71–74, (URL ⟨http://www.sciencedirect.com/science/article/pii/S0031018211001799⟩).

Meredith, M.P., King, J.C., 2005. Rapid climate change in the ocean west of the Antarctic Peninsula during the second half of the 20th century. Geophys. Res. Lett. 32 (19), L19604, (URL http://doi.wiley.com/10.1029/2005GL024042).

Meredith, M.P., Murphy, E.J., Hawker, E.J., King, J.C., Wallace, M.I., 2008. On the interannual variability of ocean temperatures around South Georgia, southern ocean: forcing by El Niño/southern oscillation and the Southern Annular Mode. Deep-Sea Res. Part II: Top. Stud. Oceanogr. 55 (18–19), 2007–2022.

Meredith, M.P., Stammerjohn, S.E., Venables, H.J., Ducklow, H.W., Martinson, D.G., Iannuzzi, R.A., Leng, M.J., Van Wessem, J.M., Reijmer, C.H., Barrand, N.E., 2016. Deep-sea research II changing distributions of sea ice melt and meteoric water west of the Antarctic Peninsula. Deep-Sea Res. Part II, 1–18, (URL ⟨http://dx.doi.org/10.1016/j.dsr2.2016.04.019⟩).

Meredith, M.P., Venables, H.J., Clarke, A., Ducklow, H.W., Erickson, M., Leng, M.J., Lenaerts, J.T.M., van den Broeke, M.R., 2013. The freshwater system west of the Antarctic Peninsula: spatial and temporal changes. J. Clim. 26 (5), 1669–1684, (URL ⟨http://journals.ametsoc.org/doi/abs/10.1175/JCLI-D-12-00246.1⟩).

Meredith, M.P., Wallace, M.I., Stammerjohn, S.E., Renfrew, I.A., Clarke, A., Venables, H.J., Shoosmith, D.R., Souster, T., Leng, M.J., 2010. Changes in the freshwater composition of the upper ocean west of the Antarctic Peninsula during the first decade of the 21st century. Prog. Oceanogr. 87 (1–4), 127–143, (URL ⟨http://www.sciencedirect.com/science/article/pii/S007966111000131X⟩).

Moffat, C., Beardsley, R.C., Owens, B., van Lipzig, N., 2008. A first description of the Antarctic Peninsula coastal current. Deep Sea Res. Part II: Top. Stud. Oceanogr. 55 (3), 277–293.

Montes-Hugo, M., Doney, S.C., Ducklow, H.W., Fraser, W., Martinson, D., Stammerjohn, S.E., Schofield, O., 2009. Recent changes in phytoplankton communities associated with rapid regional climate change along the Western Antarctic Peninsula. Science 323 (March), 1470–1473.

Nicolas, J.P., Bromwich, D.H., 2011. Precipitation changes in high southern latitudes from global reanalyses: a cautionary tale. Surv. Geophys. 32 (4–5), 475–494, (URL ⟨http://link.springer.com/10.1007/s10712-011-9114-6⟩).

Pritchard, H.D., Arthern, R.J., Vaughan, D.G., Edwards, L.A., 2009. Extensive dynamic thinning on the margins of the Greenland and Antarctic ice sheets. Nature 461 (7266), 971–975, (URL http://dx.doi.org/10.1038/nature08471).

Pritchard, H.D., Ligtenberg, S.R.M., Fricker, H.A., Vaughan, D.G., Van den Broeke, M.R., Padman, L., 2012. Antarctic ice-sheet loss driven by basal melting of ice shelves. Nature 484 (7395), 502–505, (URL ⟨http://www.ncbi.nlm.nih.gov/pubmed/22538614⟩).

Rye, C.D., Naveira Garabato, A.C., Holland, P.R., Meredith, M.P., George Nurser, A.J., Hughes, C.W., Coward, A.C., Webb, D.J., 2014. Rapid sea-level rise along the Antarctic margins in response to increased glacial discharge. Nat. Geosci. 7 (10), 732–735, (URL http://dx.doi.org/10.1038/ngeo2230).

Scambos, T., Fricker, H.A., Liu, C.-C., Bohlander, J., Fastook, J., Sargent, A., Massom, R., Wu, A.-M., 2009. Ice shelf disintegration by plate bending and hydro-fracture: satellite observations and model results of the 2008 Wilkins ice shelf break-ups. Earth Planet. Sci. Lett. 280 (1–4), 51–60, (URL ⟨http://linkinghub.elsevier.com/retrieve/pii/S0012821X08007887⟩).

Scambos, T.A., Berthier, E., Haran, T., Shuman, C.A., Cook, A.J., Ligtenberg, S.R.M., Bohlander, J., 2014. Detailed ice loss pattern in the northern Antarctic Peninsula: widespread decline driven by ice front retreats. Cryosphere 8 (6), 2135–2145, (URL ⟨http://www.the-cryosphere.net/8/2135/2014/⟩).

Schmidtko, S., Heywood, K.J., Thompson, A.F., Aoki, S., 2014. Multidecadal warming of Antarctic waters. Science 346 (6214), 1227–1231, (URL ⟨http://www.sciencemag.org/content/346/6214/1227.short⟩).

Silva, T.A.M., Bigg, G.R., Nicholls, K.W., 2006. Contribution of giant icebergs to the southern ocean freshwater flux. J. Geophys. Res. 111 (C3), C03004, (URL ⟨http://doi.wiley.com/10.1029/2004JC002843⟩).

Stammerjohn, S., Maksym, T., Heil, P., Massom, R.A., Vancoppenolle, M., Leonard, K.C., 2011. The influence of winds, sea-surface temperature and precipitation anomalies on Antarctic regional sea-ice conditions during IPY 2007. Deep Sea Res. Part II: Top. Stud. Oceanogr. 58 (9–10), 999–1018, (URL ⟨http://www.sciencedirect.com/science/article/pii/S0967064510003048⟩).

Stammerjohn, S.E., Martinson, D.G., Smith, R.C., Iannuzzi, R.A., 2008. Sea ice in the western Antarctic Peninsula region: spatio-temporal variability from ecological and climate change perspectives. Deep Sea Res. Part II: Top. Stud. Oceanogr. 55 (18–19), 2041–2058, (URL ⟨http://www.sciencedirect.com/science/article/pii/S0967064508001562⟩).

Thomas, E.R., Marshall, G.J., McConnell, J.R., 2008. A doubling in snow accumulation in the western Antarctic Peninsula. Geophys. Res. Lett. 35 (1), 1–5, (URL ⟨http://www.agu.org/pubs/crossref/2008/2007GL032529.shtml⟩).

Thompson, D.W.J., 2002. Interpretation of recent southern hemisphere climate change. Science 296 (5569), 895–899, (URL ⟨http://www.sciencemag.org/content/296/5569/895.short⟩).

Turner, J., 2004. The El Niño southern oscillation and Antarctica. Int. J. Climatol. 24 (1), 1–31, (URL http://doi.wiley.com/10.1002/joc.965).

Van Lipzig, N.P.M., King, J.C., Lachlan-Cope, T.A., 2004. Precipitation, sublimation, and snow drift in the Antarctic Peninsula region from a regional atmospheric model. J. Geophys. Res. 109 (D24), 1–16, (URL ⟨http://www.agu.org/pubs/crossref/2004/2004JD004701.shtml⟩).

van Lipzig, N.P.M., Marshall, G.J., Orr, A., King, J.C., 2008. The relationship between the southern hemisphere annular mode and Antarctic peninsula summer temperatures: analysis of a high-resolution model climatology. J. Clim. 21 (8), 1649–1668, (URL ⟨http://journals.ametsoc.org/doi/abs/10.1175/2007JCLI1695.1⟩).

Van Wessem, J.M., Ligtenberg, S.R.M., Reijmer, C.H., Van de Berg, W.J., Van den Broeke, M.R., Barrand, N.E., Thomas, E.R., Turner, J., Wuite, J., Scambos, T.A., Van Meijgaard, E., 2016. The modelled surface mass balance of the Antarctic Peninsula at 5.5 km horizontal resolution. Cryosphere 10 (1), 271–285, (URL ⟨http://www.the-cryosphere.net/10/271/2016/⟩).

Van Wessem, J.M., Reijmer, C.H., Lenaerts, J.T.M., Van de Berg, W.J., Van den Broeke, M.R., Van Meijgaard, E., 2014a. Updated cloud physics in a regional atmospheric climate model improves the modelled surface energy balance of Antarctica. Cryosphere 8 (1), 125–135, (URL ⟨http://www.the-cryosphere.net/8/125/2014/⟩).

Van Wessem, J.M., Reijmer, C.H., Morlighem, M., Mouginot, J., Rignot, E., Medley, B., Joughin, I., Wouters, B., Depoorter, M.A., Bamber, J.L., Lenaerts, J.T.M., Van De Berg, W.J., Van Den Broeke, M.R., Van Meijgaard, E., 2014b. Improved representation of East Antarctic surface mass balance in a regional atmospheric climate model. J. Glaciol. 60 (224), 761–770, (URL ⟨http://www.igsoc.org/journal/60/222/t14j051.html⟩).

Van Wessem, J.M., Reijmer, C.H., Van de Berg, W.J., Van den Broeke, M.R., Cook, A.J., Van Ulft, L.H., Van Meijgaard, E., 2015. Temperature and wind climate of the Antarctic Peninsula as simulated by a high-resolution regional atmospheric climate model. J. Clim. 28 (18), 7306–7326, (URL ⟨http://journals.ametsoc.org/doi/abs/10.1175/JCLI-D-15-0060.1⟩).

Vaughan, D.G., 2006. Recent trends in melting conditions on the Antarctic Peninsula and their implications for ice-sheet mass balance and sea level. Arct., Antarct., Alp. Res. 38 (1), 147–152.

Vaughan, D.G., Marshall, G., Connolley, W.M., Parkinson, C., Mulvaney, R., Hodgson, D.A., King, J.C., Pudsey, C.J., Turner, J., 2003. Recent rapid regional climate warming on the Antarctic Peninsula. Clim. Change 60, 243–274.

Wolter, K., Timlin, M., 1993. Monitoring ENSO in COADS with a seasonally adjusted principal component index. In: Proceedings of the 17th Climate Diagnostics. (URL ⟨http://140.172.38.100/psd/enso/mei.ext/WT1.pdf⟩).

Wouters, B., Martin-Español, A., Helm, V., Flament, T., van Wessem, J.M., Ligtenberg, S.R.M., van den Broeke, M.R., Bamber, J.L., 2015. Dynamic thinning of glaciers on the Southern Antarctic Peninsula. Science 348 (6237), 899–903, (URL ⟨http://www.sciencemag.org/content/348/6237/899.abstract⟩).

Yuan, X., 2004. ENSO-related impacts on Antarctic sea ice: a synthesis of phenomenon and mechanisms. Antarct. Sci. 16 (4), 415–425, (URL ⟨http://journals.cambridge.org/abstract_S0954102004002238⟩).